Critical-velocity effects in vibrating superleaks: Vortex nucleation processes

Paul Muzikar and N. Giordano
Department of Physics, Purdue University, West Lafayette, Indiana 47907
(Received 8 January 1986)

We develop a theory which concerns how the operation of a vibrating superleak transducer is affected by the nucleation of vortices in the pores of the superleak. At large drive amplitudes a significant chemical potential difference is established between the two sides of the superleak. As a result, both the first- and second-sound waves generated by the transducer show interesting structure. The study of this structure may provide a useful means of experimentally probing vortex nucleation processes in superfluids.

I. INTRODUCTION

The process of vortex nucleation is of fundamental importance in the physics of superfluid ^{4}He. In particular, the generation of vortices can degrade a supercurrent; this illustrates the metastable nature of superflow, and provides a mechanism to account for the critical velocity of the fluid. Detailed theories, such as the Langer-Fisher homogeneous nucleation theory,[1] represent attempts to make these ideas quantitative. Various experiments have given support to this theory, but it seems fair to say that the overall understanding of this phenomenon is far from complete.

In this paper we explore how vibrating superleak transducers (VSTs) are affected by vortex nucleation. These transducers are simple capacitive microphones/speakers, in which the vibrating element is a superleak. They were invented a number of years ago,[2,3] and are now widely used to generate and detect second-sound in superfluids. These transducers have recently attracted a good deal of theoretical and experimental attention,[4–15] and there is now a fairly complete understanding of how they function in the limit that the intensity of the generated sound is small. It turns out that the superfluid velocity can become quite large in the pores of the superleak membrane in a VST, and hence these pores are a prime location for the creation of vortices. Since the region in which the superfluid velocity is large is limited to the pores of the superleak, the vortex nucleation processes are also limited to this region. This makes VSTs ideal, in some respects, for the study of these sorts of processes. In this paper we give a general discussion of how the equations governing the behavior of VSTs are modified by vortex nucleation effects; in addition, the limits of validity of the new equations are carefully assessed. While the new equations are not terribly complicated in form, it is necessary to solve them numerically, and we also present and discuss some illustrative numerical results. We find that when the driving force on the superleak of the VST is sufficiently large, several dramatic effects occur. First, the waveform of the generated second-sound becomes very distorted, and its amplitude saturates. Second, the generated first-sound acquires a wild oscillation on a very short time scale. These findings are also compared with some recent experimental results.

The work presented here is of interest for two reasons. On the one hand, it is important to understand how these transducers work, so that they can be used wisely for various purposes. Recent research has indeed greatly clarified our picture of how they function in the limit that the driving force, and hence the generated sound intensity, is small. One of the goals of the present work is to extend this understanding to the regime in which the nonlinearities caused by vortex nucleation processes are important. In addition, the vortex nucleation processes involved in the transducer operation are themselves of great interest. Indeed, VSTs may provide a convenient tool with which to study these processes.

The plan of this paper is as follows. In Sec. II we derive the equations of motion for the superleak membrane of a VST, including the effects of vortex nucleation. In Sec. III we present some results obtained by numerically integrating the equations of motion. Section IV contains a discussion and summary. We will follow as closely as possible the notation of Ref. 7. Note that in the present work we are studying only the generation, not the detection, of sound. A preliminary account of some of this work has already appeared.[10]

II. EQUATIONS OF MOTION

In this section we explain how to incorporate the effects of vortex nucleation into the equations of motion of the VST. If we ignore these effects, the two fundamental equations are (15) and (32) of Ref. 7. These equations describe VST behavior in the linear regime (i.e., the regime in which vortex nucleation effects are not important). In this case the driving force and the amplitudes of the generated first- and second-sound waves are small, and these amplitudes are proportional to the driving force. Equation (15) in Ref. 7 expresses the fact that, in the absence of any dissipative processes within the pores of the superleak, the chemical potential is the same on both sides of the superleak. Equation (32) is simply a version of Hooke's law, expressing momentum conservation. How must these two equations be modified for our present pur-

pose?

We first review our notation. The superfluid and normal fluid velocities at the membrane are denoted by v_s and v_n. The velocity of the membrane is also v_n, since we are assuming that the Poiseuille flow of the normal component is negligible. We also define x_n and x_s, the displacements of the normal and superfluid components; these satisfy $v_s=\dot{x}_s$ and $v_n=\dot{x}_n$. The first-sound amplitude, v, and the second-sound amplitude w, are given by

$$v=\frac{\rho_n v_n+\rho_s v_s}{\rho} , \tag{1}$$

$$w=\frac{\rho_s}{\rho}(v_n-v_s) , \tag{2}$$

where ρ_s, ρ_n, and ρ are the superfluid, normal, and total densities. Finally we define y and z by $\dot{y}=v$ and $\dot{z}=w$, so that

$$y=\frac{\rho_n x_n+\rho_s x_s}{\rho} , \tag{3}$$

$$z=\frac{\rho_s}{\rho}(x_n-x_s) . \tag{4}$$

We now argue that the main effect of vortex nucleation processes is to create a nonzero chemical potential difference between the two sides of the superleak membrane. We model this effect by modifying Eq. (3) of Ref. 7 to

$$\delta\mu_b-\delta\mu_c=\mathrm{sgn}(v_s-v_n)D\exp\left[\frac{-B\alpha}{|v_s-v_n|}\right] , \tag{5}$$

which is essentially the Langer-Fisher result. Here,

$$D=\frac{h}{M}V_p f_0 , \tag{6}$$

where V_p is the volume of a pore in the membrane, f_0 is the number of nucleation attempts per unit volume per unit time, h is Planck's constant, α is the porosity, and M is the ^{4}He mass. The parameter f_0 is difficult to estimate theoretically, and we will rely on previous experimental results[16] to select an appropriate value. The quantity B appearing in the exponent is given by

$$B=\frac{\theta\rho_s}{\rho kT} , \tag{7}$$

where θ is a parameter we will also take from previous experiments.[16]

The specific expression for the chemical potential difference is taken from the Langer-Fisher homogeneous nucleation theory, and one might therefore ask how sensitive our results are to uncertainties, assumptions, etc., in the Langer-Fisher theory. Langer and Reppy[17] have shown, using very general arguments, that the functional forms in (5) and (7), and in particular the dependence of $\delta\mu$ on both ρ_s and $|v_s-v_n|$, follow quite naturally from any homogeneous vortex nucleation type of theory. Moreover, we would expect that *any* mechanism which yields a critical velocity should lead to a result quantitatively similar to (5). Hence, our calculations should give a good indication of the behavior to be expected, regardless of the details of the dominant dissipative process.

The other basic equation we need concerns the momentum conservation law for the superleak. This is not affected by vortex nucleation effects, and thus Eq. (32) of Ref. 7 remains unchanged:

$$M_m^*\dot{v}_n+M_s^*\dot{v}_s=-Kx_n-A\rho\left[\frac{c_1^2}{L}y+c_1 v\right]+f(t) . \tag{8}$$

Here, $f(t)$ is the applied driving force, A the area of the membrane, c_1 the first-sound velocity, K the spring constant of the membrane, and the two effective masses are given by

$$M_m^*=V_m[(\rho_m-\rho_s)(1-\alpha)+\rho_n\alpha] , \tag{9}$$

$$M_s^*=V_m\rho_s , \tag{10}$$

where V_m is the membrane volume.

Our final set of coupled equations, in terms of the variables v, w, y and z is

$$\dot{y}=v , \tag{11}$$

$$\dot{z}=w , \tag{12}$$

$$\frac{\rho_n}{\rho_s}c_2 w-c_1 v+\frac{\rho_n c_2^2 z}{\rho_s L}-\frac{c_1^2 y}{L}=-\mathrm{sgn}(w)D\exp\left[\frac{\rho_s^2\theta\alpha}{\rho^2 kT|w|}\right] , \tag{13}$$

$$\left[M_m^*+M_s^*\right]\dot{v}+\left[M_m^*-\frac{\rho_n}{\rho_s}M_s^*\right]\dot{w}=-K(y+z)-A\rho\left[\frac{c_1^2 y}{L}+c_1 v\right]+f(t) . \tag{14}$$

Here c_2 is the velocity of second sound. In the next section we will show some representative numerical solutions to the above set of coupled equations; in particular, we will show $v(t)$ and $w(t)$ for sinusoidal driving forces of various amplitudes. We conclude this section with a discussion of the limits of validity of our equations.

Because various quantities, such as ρ, v, and w, were taken to be spatially uniform in the backplate region, we must have the wavelengths of first- and second-sound larger than L, the distance between the membrane and the backplate.[6] This means that our equations are strictly valid only for time scales longer than either L/c_1 or L/c_2. In addition, we have ignored the possibility of fourth-sound propagation through the pores;[6] this implies that our equations are valid only for time scales longer than L_m/c_4, where L_m is the thickness of the membrane and c_4 is the fourth-sound velocity. Thus, we can only study phenomena with a time scale τ satisfying

$$\tau>\max\left[\frac{L}{c_1},\frac{L}{c_2},\frac{L_m}{c_4}\right] . \tag{15}$$

Features we find on time scales shorter than τ may still represent real effects, but these equations cannot provide a complete description of the behavior on such time scales.

TABLE I. Values of VST parameters.

Parameter	Value
A (cm^2)	1.77
K ($g\ s^{-2}$)	10^8
f_0 ($cm^{-3}\ s^{-1}$)	5×10^{27}
θ ($g\ cm^3\ s^{-3}$)	1.3×10^{-12}
ρ ($g\ cm^{-3}$)	0.14
L_m (cm)	5×10^{-4}
ρ_m ($g\ cm^{-3}$)	0.95

III. RESULTS

We have numerically solved Eqs. (11)–(14) for a variety of cases with a driving force of the form $f(t)=F\sin(\omega t)$. (See the Appendix for details on how we solved the equations.) For small enough F one is below the critical velocity regime. In this case vortex creation processes are unimportant, and $v(t)$ and $w(t)$ were found to be sinusoidal with maximum amplitudes related by the theoretically expected ratio:[4–6]

$$\frac{v_{\max}}{w_{\max}}=\frac{\rho_n c_2^2}{\rho_s c_1^2}\ . \tag{16}$$

Moreover, the overall amplitudes of the generated first- and second-sound waves were in perfect agreement with the theory which is applicable in the linear regime.[7] As we increase F the quantity $|v_s-v_n|$ in the pores becomes very large, and the nonlinear term in the equations becomes important.

A choice must be made of what values to assign to the many constants appearing in the equations. We tried to pick values appropriate for typical experimental situations. For all of our runs we chose $\alpha=0.012$ and a pore diameter of 500 Å. The small diameter makes the Poiseuille flow through the pores negligible,[4,7,18] and the small size of α makes the superfluid velocity through the pores large. Besides α and the pore diameter, various other constants were held fixed for all of our runs; Table I lists their values. These values are appropriate for a VST which follows the now standard design,[13,7] and which employs a nuclepore filter membrane as the superleak. Finally, we note that our results are clearly very sensitive to the size of θ, since it appears in the exponent of the nonlinear term, and essentially determines when the vortex nucleation processes become important.

TABLE II. Parameters for data sets *A*, *B*, and *C*.

Parameter	A	B	C
ρ_s/ρ	0.0441	0.8548	0.0441
c_1 (cm/s)	2.2×10^4	2.37×10^4	2.2×10^4
c_2 (cm/s)	452	1855	452
T (K)	2.17	1.2	2.17
L (cm)	2×10^{-3}	2×10^{-3}	2×10^{-4}
$\omega/2\pi$ (s^{-1})	4×10^3	4×10^3	2×10^4
c_4 (cm/s)	4.6×10^3	2.2×10^4	4.6×10^3

The remaining parameters were varied as we did our calculations. For three different sets of calculations, which we will call *A*, *B*, and *C*, the remaining parameters had the values listed in Table II. The parameters for sets *A* and *C* are chosen such that the temperature is very close to the λ point, while set *B* is chosen such that it is very far away.

Figure 1 shows $w(t)$ for various values of F, with parameters from set A being used; Fig. 2 shows the corresponding results for $v(t)$. By about $F\cong150$ (note that the units here are cgs, so that F is in dyn/cm^2 throughout), $w(t)$ shows deviations from a purely sinusoidal shape, and its amplitude is no longer increasing linearly with F. At $F\cong2000$, $w(t)$ has become quite close to a square wave. Figure 3 shows a plot, on a blown up time scale, of the rapid variation in time which occurs in $w(t)$ for $F=2000$.

The behavior of $v(t)$ is quite different. Its overall shape is not very distorted at higher values of F, and its magnitude still increases approximately linearly[19] with F. However, a "glitch" appears near the maximum; on a very short time scale $v(t)$ attains a very large amplitude, and then settles back into its smoother overall motion. The time scales on Fig. 2 are too coarse to show this glitch accurately. Figure 4 displays the glitch's shape on a much finer time scale.

For data set *B*, which has values of the temperature-dependent parameters appropriate for T far from the λ point, the nonlinear effect sets in at about $F\cong30\,000$. Figure 5 shows $w(t)$ and $v(t)$ for $F=10^5$, while Fig. 6 shows the interesting structure in $v(t)$ on a finer scale.

The large jump over a very short time scale exhibited by $v(t)$ is clearly of interest. One problem with data sets A and B is that this fine structure occurs over a time scale which is shorter than the limits set by (15). The weak point is that L/c_2 is too long. Hence it is not clear to what extent the fine structure could be changed by other effects.

In an effort to examine this problem we chose L in data set *C* to be ten times smaller than in *A* or *B*; for convenience, we also chose a higher drive frequency. Figure 7 shows $v(t)$ and $w(t)$ with parameters from data set *C*. Figure 8 shows the interesting structure in $v(t)$ on a finer scale. For this data set, the quantity τ in (15) is about 4×10^{-7} s. An examination of Fig. 8 shows that the glitch in $v(t)$ occurs over a time longer than this. So we believe the glitch is a real effect; the fact that it occurs around the time that $w(t)$ is going through a drastic change is reasonable, since $v(t)$ and $w(t)$ are intimately coupled by the equations. The glitch can be understood quantitatively in the following manner. If we assume a square-wave-type behavior for $w(t)$ (as seen in Fig. 1 for large values of F) then the term involving $\dot{w}$ in (14) will be extremely large when $w(t)$ passes through zero (Fig. 3). Equation (14) can then be viewed as an equation of motion for $v(t)$, with the term involving $\dot{w}$ acting like a large driving force. This large force acts over a very short time, and thus imparts an impulse to $v(t)$. In response to this impulse $v(t)$ "rings" at its natural frequency, and this frequency can be estimated from (14). For the parameters of data set *A*, the natural frequency for $v(t)$ is approximately 1×10^6 Hz, and this agrees fairly well with the os-

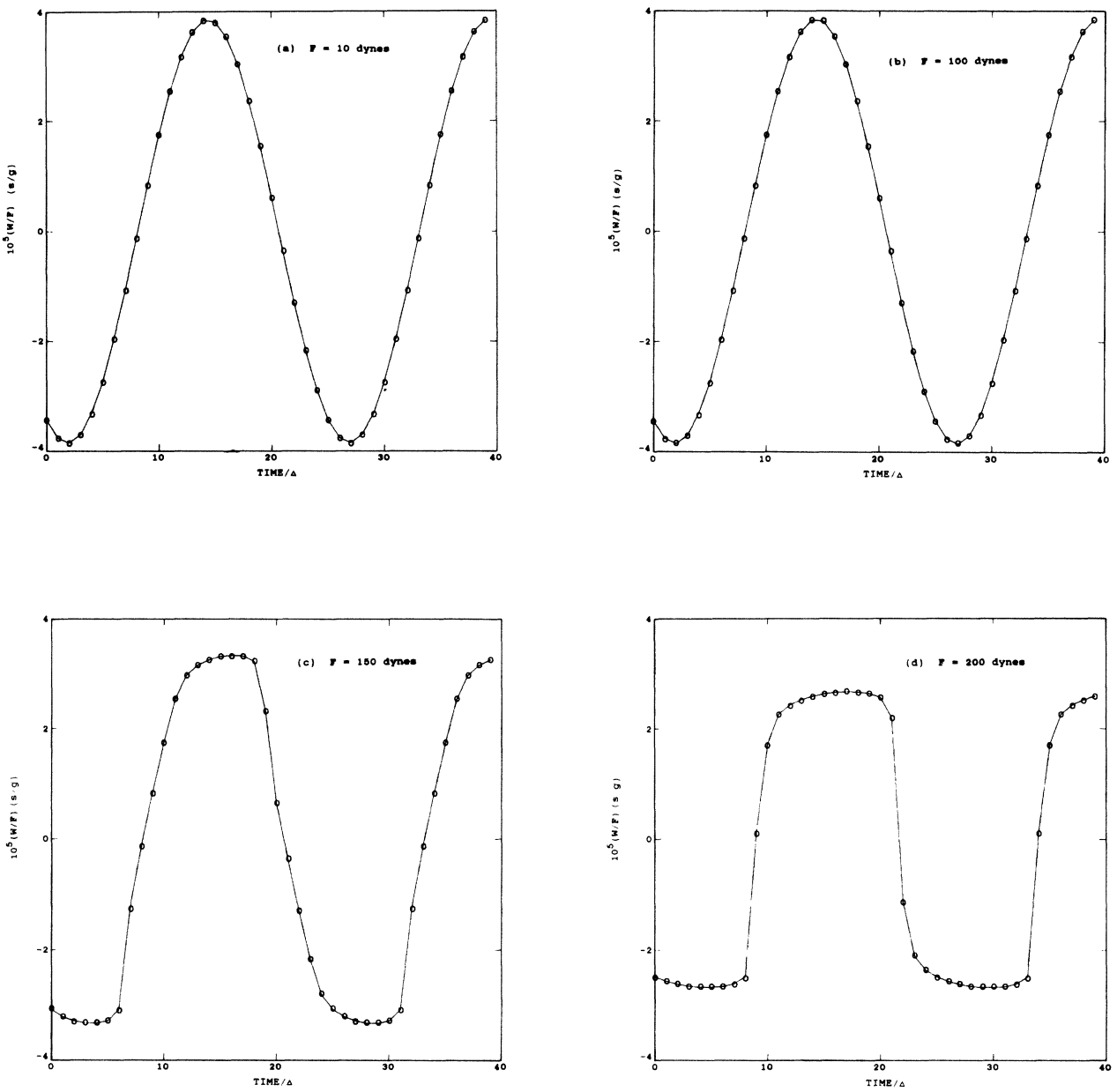

FIG. 1. Generated second-sound wave for a series of drive amplitudes. Each unit of time, Δ, represents 10^{-5} s, and the parameters of data set A are used. Note that the vertical scale is not the same in each plot, and that $w(t)$ is normalized by F, the drive amplitude. Every hundredth computed point is represented by a O (i.e., there are 99 computed points between each plotted point, but for clarity they are not shown). The time step for this computation was 10^{-7} s, and hence the *total* time interval shown is 4×10^{-4} s.

cillation frequency seen in Fig. 4. In addition, the damping can be estimated from the imaginary part of the natural frequency, and from (14) we find that the imaginary part is about half the size of the real part. Thus we expect the ringing to last for about two periods before it is damped out, and this is also in good agreement with the behavior seen in Fig. 4.

Our calculations allow us to study the maximum displacement of the membrane, ΔL; the membrane displacement is given by $y(t)+z(t)$. For data set A the membrane displacement, even deeply into the nonlinear regime, is very small. For example, at $F=2000$, $\Delta L/L$ is of the order 10^{-4}. However, at the lower temperatures it takes a larger F to see the vortex creation effects. The ratio $\Delta L/L$ is then quite a bit larger when we enter critical velocity region. For data set B, at $F=50000$, $\Delta L/L\cong0.14$. We also note that if we double F to 10^5, $\Delta L/L$ only increases to about 0.16; as expected, vortex nucleation makes the transducer much stiffer. Finally, for data set C and $F=2000$, $\Delta L/L\cong3\times10^{-4}$. Figure 9

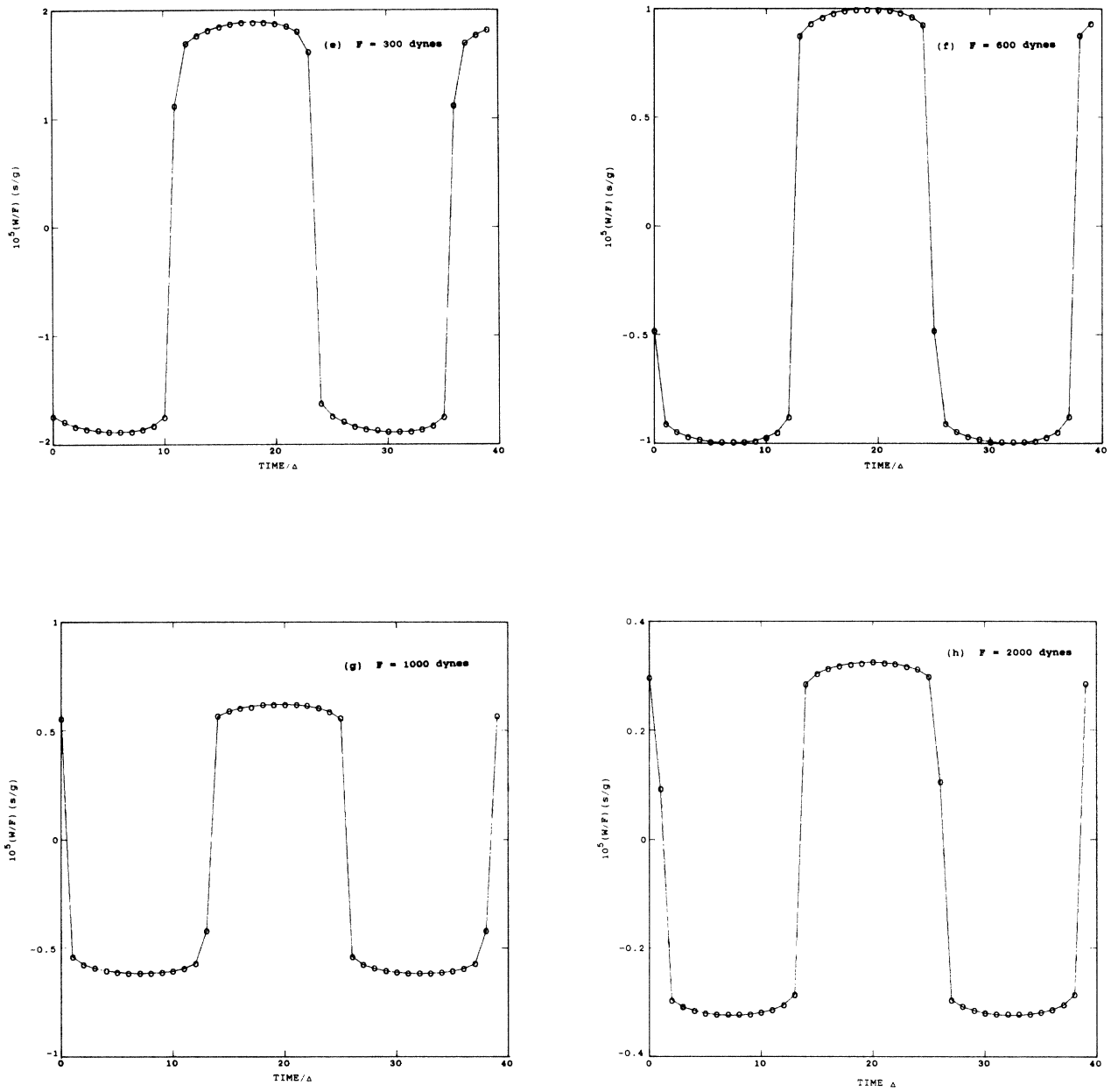

FIG. 1. (*Continued*).

shows a plot of the membrane displacement versus time for data set B and $F=10^6$.

Again, we should stress that effects such as the flat top developed in $w(t)$ are not put in by hand, but emerge naturally from our coupled set of equations.

IV. DISCUSSION

Our goal in this work was to examine the effect of vortex nucleation in the superleak on the behavior of a VST. To this end we developed the relatively simple set of equations, (11)—(14). The chemical potential difference between the front and back of the membrane grows as the quantity $|v_s - v_n|$ grows. This chemical potential difference feeds into the equations of motion, and leads to interesting effects in both the first- and second-sound which is generated. The "flat-topped" structure appearing in $w(t)$ is what one would intuitively expect as a critical velocity effect. In our work, this structure is not put in by hand, but emerges naturally from the equations. The glitch which develops in $v(t)$ is more difficult to understand physically, although as noted above, the "mathematical" origin is not hard to see.

In comparing our theory with experiment, several points should be borne in mind. The extent to which oth-

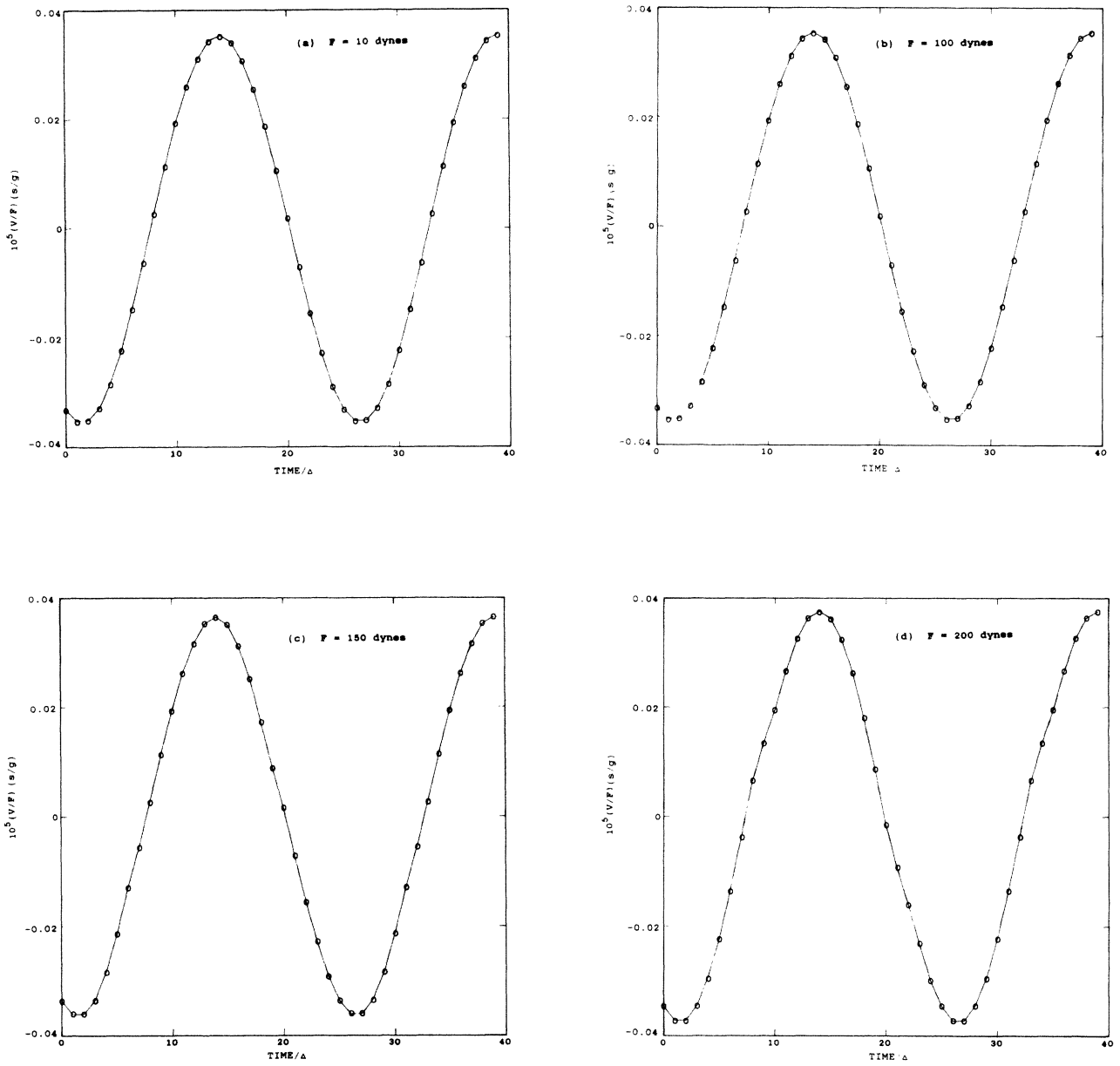

FIG. 2. Generated first-sound wave for a series of drive amplitudes. All of the parameters are the same as in Fig. 1. The time scales in Figs. 1 and 2 have the *same* zeros, so the relative sizes of $v(t)$ and $w(t)$ at various times can be compared directly. As in Fig. 1, only every hundredth computed point is shown. The glitch appearing at large drive amplitudes is not accurately represented on the coarse time scale of this plot, because the time interval between neighboring points is comparable to the total duration of the glitch. When examined on a very fine time scale (as in Figs. 4, 6, and 8) the glitch is found to display the expected symmetry with respect to the period of the driving force.

er nonlinear effects are important is not clear. These other effects could include, for example, terms in the hydrodynamic equations which are second order in the deviation of the fluid from equilibrium. In addition, forms other than the Langer-Fisher form for the chemical potential difference are conceivable; for example our vortices are nucleating in the finite-sized pores, so the homogeneous nucleation theory may not be totally appropriate.[20] Finally, most of the experiments are performed with the VSTs located at the ends of a resonant cavity, but the effects of such a cavity are not included in our theory.

Experimental results[9,11] are available for parameters similar to our set A. The calculations indicate that for this case the nonlinearities set in at about $F=150$. The

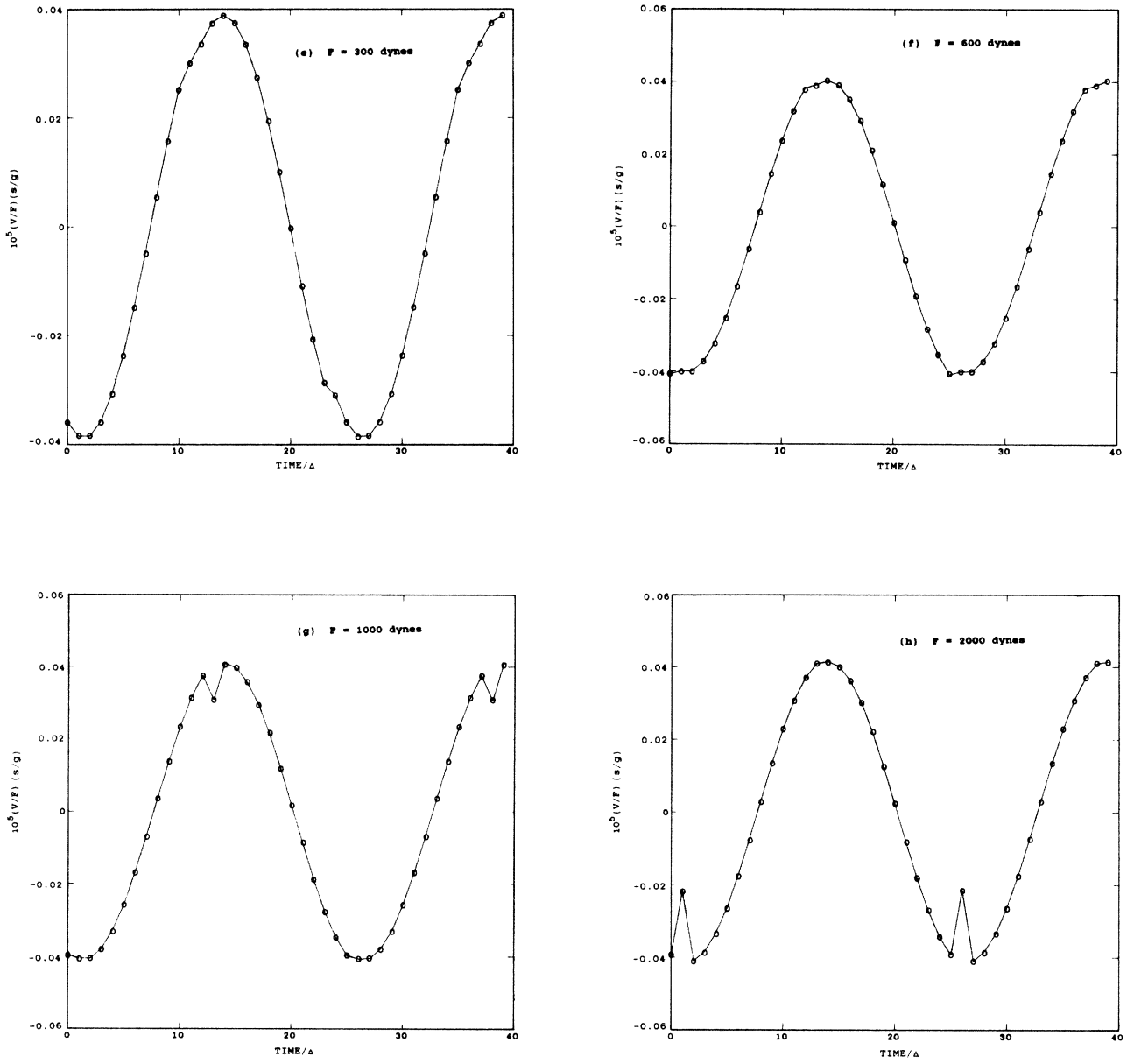

FIG. 2. (*Continued*).

experiments[11] find that this occurs at about $F=10$. Given all of the uncertainties in the parameters which are involved in both the experiments and the theory (especially in the parameter θ in the latter), this level of agreement is probably all that could be expected. Note that the experiments were performed in a resonant cavity geometry, although it has been argued[11] that this should not affect the relationship between F and $w(t)$. An interesting finding in the experiments was that the generated second-sound wave possessed harmonic components at both odd and even multiples of the driving frequency. Our calculations yield essentially "square" waves for w, and these contain only odd multiples of the drive frequency. This is a potentially serious discrepancy whose origin is not understood. It could conceivably be due to the effect of the resonant cavity on the experiment. However we have performed some preliminary calculations which include these effects, and which still yield only odd frequency components. The discrepancy could also be due to a fundamental problem with the form of the dissipative term in our basic equations, but as we have argued above, it is hard to see how any mechanism which yields a critical velocity would lead to a term with a significantly different form. Further work on this problem is certainly of interest.

It is appropriate at this point to discuss the work of Grabinski and Liu,[12] who also have considered critical velocity effects in VSTs. While their paper contains an

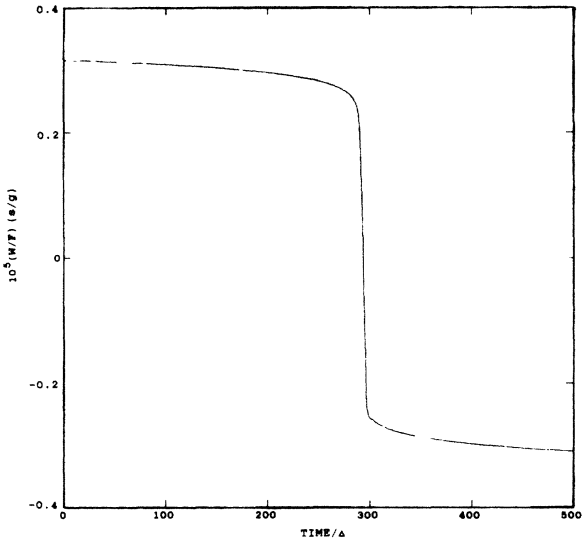

FIG. 3. Second-sound wave for a drive amplitude F of 2000, with parameters taken from data set A. Each unit of time, Δ, represents 10^{-7} s. This plot focuses on the time interval during which $w(t)$ goes through a sudden change. Note that the entire time interval shown is only 5×10^{-5} s, while the driving period is 5×10^{-4} s.

instructive and intuitive analysis, we should raise several points. In contrast to our calculations, these authors do not consider at all the force on the membrane in their calculations. Rather, they obtain relationships between the membrane displacement and other quantities such as v_m, w, and v. In addition, critical velocity effects are put in "by hand." That is, it is assumed that the behavior becomes "critical" when v_s in the pores exceeds a certain value; the relationship between v_s and $\delta\mu$, (5), does not enter.

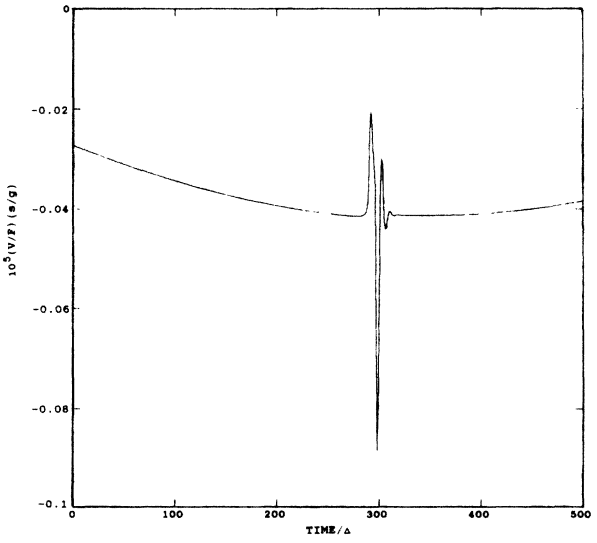

FIG. 4. First-sound wave for the same parameters and time scales as in Fig. 3. The time scales in Figs. 3 and 4 have the *same* zeros. Note that the glitch in $v(t)$ occurs at the time that $w(t)$ goes through its abrupt change.

The results of Grabinski and Liu are in many ways complementary to ours. They have the advantage of being analytical, but since the driving force does not enter, it is difficult to compare them directly to experimental observations. While it is possible, at least in principle, to imagine an experimental arrangement in which the driving force is varied in a manner such that a particular membrane displacement is obtained, it is not clear how easy this would be in practice. As we have seen above, in

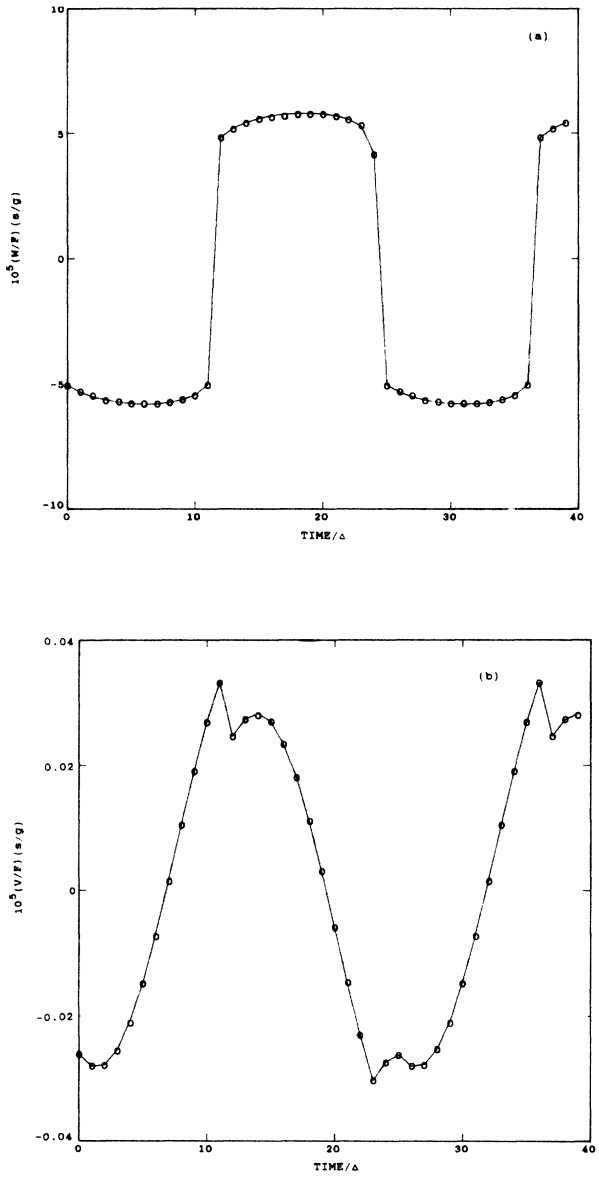

FIG. 5. (a) Second-sound and (b) first-sound waves for data set B, with $F=10^5$. One unit of time, Δ, represents 10^{-5} s. The glitch appearing at large drive amplitudes is not accurately represented on the coarse time scale of this plot, because the time interval between neighboring points is comparable to the total duration of the glitch. When examined on a very fine time scale (as in Figs. 4, 6, and 8) the glitch is found to display the expected symmetry with respect to the period of the driving force.

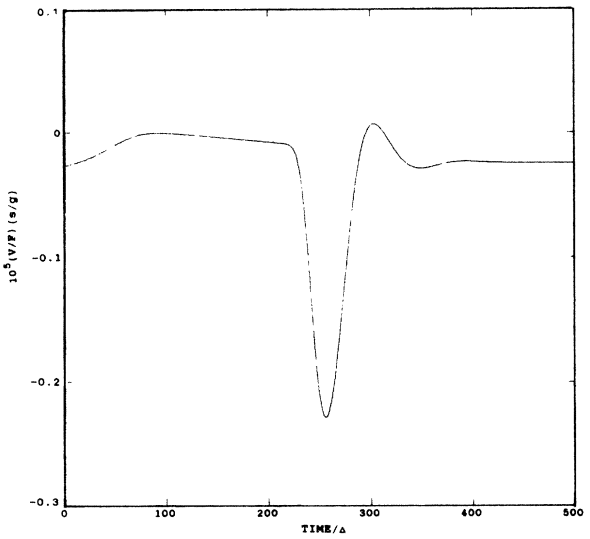

FIG. 6. Fine structure in the first-sound signal. The parameters are from data set B, and $F=10^5$. One unit of time, Δ, represents 10^{-8} s.

the vortex nucleation region large increases in the force cause only very small increases in the membrane displacement. Enormous, and perhaps impractically large (and of course, extremely non-sinusoidal) forces would be required to carry out such a scheme. It is also hard to see how the approach of Grabinski and Liu could be used to study critical velocity effects quantitatively, since their calculations, at least in their present form, do not include the $v_s(\delta\mu)$ relationship at all.

We should also note that Grabinski and Liu have attributed the presence of both odd and even overtones in the experiments (as discussed above) to effects nonlinear in $\Delta L/L$, which seems quite reasonable. They have also proposed that this quantity becomes large in typical VSTs so that terms of order $(\Delta L/L)^2$ must be included in the equation of motion. Such effects are not included in our calculations. However, as mentioned in Sec. III, our results indicate that at least in VSTs with the "ideal" geometry which we have considered in our calculations, $\Delta L/L$ is generally quite small, even in the nonlinear regime. For example, for data set A it is roughly 10^{-4} for the largest driving forces we employed. Hence their explanation does not seem feasible for the ideal case, unless, for example, the parameter θ has a much larger value than we have assumed (and has been found in previous experiments[16]). It seems more likely that other effects, such as non-idealities present in real VSTs,[21] are important, and make terms of order $(\Delta L/L)^2$ appreciable.

Our work represents a first step towards understanding, in a quantitative way, the effects of vortex nucleation on

TABLE III. Eigenfrequencies (in units of s^{-1}) of the VST for data sets A, B, and C, in the limit of low drive amplitudes (i.e., when nonlinear effects are negligible). The normal modes are assumed to have a time dependence of the form $e^{(\pm i\omega t-\gamma t)}$.

Data set	ω	γ
A	1.14×10^6	4.63×10^6
	0	2.92×10^5
B	4.91×10^5	5.51×10^4
	0	1.17×10^7
C	2.24×10^6	1.71×10^6
	0	7.18×10^7

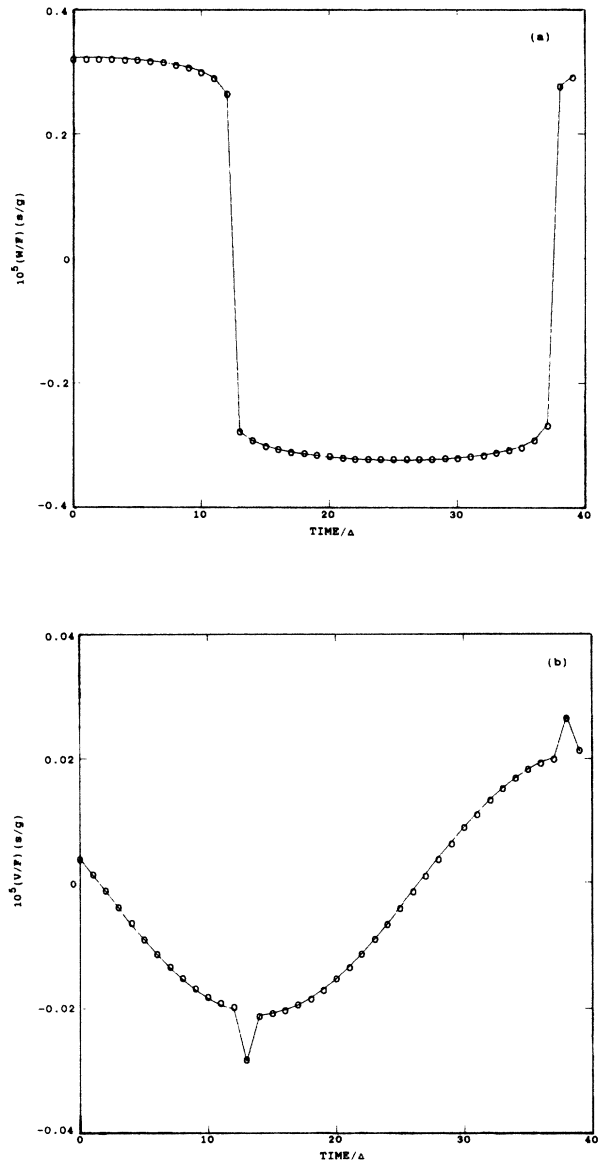

FIG. 7. (a) Second-sound and (b) first-sound waves for data set C with $F=2000$. One unit of time, Δ, represents 10^{-6} s. The glitch appearing at large drive amplitudes is not accurately represented on the coarse time scale of this plot, because the time interval between neighboring points is comparable to the total duration of the glitch. When examined on a very fine time scale (as in Figs. 4, 6, and 8) the glitch is found to display the expected symmetry with respect to the period of the driving force.

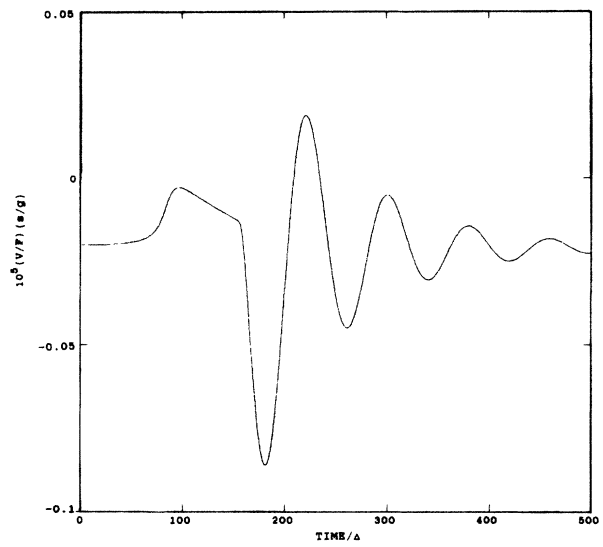

FIG. 8. Fine structure in the first-sound signal for data set C with $F=2000$. One unit of time, Δ, represents 3×10^{-9} s. This fine structure occurs in the region where the coarse grained v(t), shown in Fig. 7, is at its minimum.

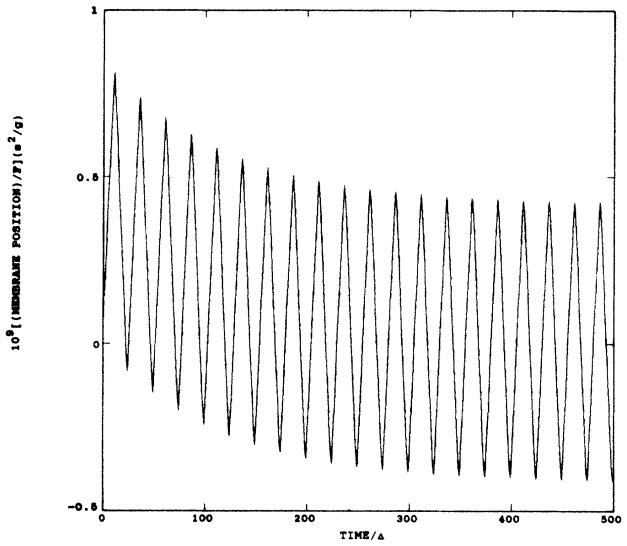

FIG. 9. Membrane displacement for data set B, with $F=10^6$. One unit of time, Δ, represents 10^{-5} s. All the variables were started at zero, and one can see the membrane relaxing to its steady-state motion as the initial transients die away.

the operation of VSTs. While our results agree, at least qualitatively, with experiments, a great deal more remains to be done. Most notable is the appearance in the experiments of even overtones of the driving frequency. It is not at all clear how to account for these theoretically. Either we do not yet understand how to treat the dissipative effects with regards to VST theory, or perhaps current ideas concerning the dissipative processes (i.e., vortex nucleation processes) are somehow incorrect. Indeed, one might hope that further experiments could, in conjunction with the theory, be used to test the validity of the precise form for the dissipative term, and determine the values of the various parameters which are involved. Hence, VSTs may well provide a very useful tool with which to study vortex nucleation effects.

It should also be noted that our basic VST relations are a coupled set of nonlinear differential equations, which are similar in form to those which have attracted a great deal of attention in the theory of chaotic systems. We have searched for chaotic solutions to our equations, but have so far been unable to find any. However, it seems entirely possible that such solutions may exist, and hence that real VSTs might exhibit chaotic behavior under the appropriate conditions. If so, VSTs may prove to be a convenient system in which to study such effects.

ACKNOWLEDGMENTS

We thank R. J. Donnelly, M. Liu, F. Pobell, W. M. Saslow, and W. Zimmermann, Jr. for stimulating discussions and correspondence. We especially thank M. Liu for insightful comments which stimulated our thinking on the origin of the glitches in $v(t)$.

APPENDIX

To numerically solve Eqs. (11)—(14), we eliminated v, and thus got the following set of three coupled first-order equations:

$$\dot{z}=w\ , \tag{A1}$$

$$\dot{y}=\gamma w+\frac{\gamma c_2 z}{L}-\frac{c_1 y}{L}+\mathrm{sgn}(w)\frac{D}{c_1}\exp\left[-\frac{c}{|w|}\right], \tag{A2}$$

$$\dot{w}=M^{-1}\left\{-K(y+z)-A\rho\frac{c_1^2}{L}y+\left[(M_s^*+M_m^*)\frac{c_1}{L}-A\rho c_1\right]*\left[\gamma w+\frac{\gamma c_2 z}{L}-\frac{c_1 y}{L}+\mathrm{sgn}(w)\frac{D}{c_1}\exp\left[\frac{-c}{|w|}\right]\right]\right.$$
$$\left.+f(t)-(M_s^*+M_m^*)\frac{\gamma c_2}{L}w\right\}, \tag{A3}$$

where

$$M \equiv M_m^* + \gamma(M_s^* + M_m^*) - \frac{\rho_n}{\rho_s} M_s^* + \frac{(M_s^* + M_m^*)cD}{c_1 w^2} \exp\left[\frac{-c}{|w|}\right], \tag{A4}$$

$$\gamma \equiv \frac{\rho_n c_2}{\rho_s c_1}, \tag{A5}$$

$$c \equiv \left[\frac{\rho_s}{\rho}\right]^2 \frac{\theta\alpha}{kT}. \tag{A6}$$

We then used a fourth-order Runge-Kutta technique to integrate forward in time, setting all the variables initially to zero. Typical step sizes in time were 10^{-7} s to 10^{-9} s. After initial transients had died away, we were left with the steady-state variation of $v(t)$ and $w(t)$. Integrating the equations through about ten periods of $f(t)$ was usually adequate to determine the steady state of v and w.

If we omit the nonlinear vortex nucleation terms from Eqs. (A1)–(A3), we are left with a linear system. The eigenfrequencies of this system, for data sets A, B and C, are listed in Table III. As can be seen, for each data set there are two heavily damped oscillating modes and one decaying mode. The values of these eigenfrequencies clearly provide a constraint on how long we can make the step size.

One drawback of our method is that the right hand side of Eq. (A2) has several large terms canceling to yield a much smaller number; this reflects the small size of v. However, our accuracy was sufficient to handle this problem.

[1]J. S. Langer and M. E. Fisher, Phys. Rev. Lett. **19**, 560 (1967).

[2]R. Williams, S. E. A. Beaver, J. C. Fraser, R. S. Kagiwada, and I. Rudnick, Phys. Lett. **29A**, 279 (1969).

[3]R. A. Sherlock and D. O. Edwards, Rev. Sci. Instrum. **41**, 1603 (1970).

[4]M. Liu and M. R. Stern, Phys. Rev. Lett. **48**, 1842 (1982); **49**, 1362 (1982).

[5]D. L. Johnson, Phys. Rev. Lett. **49**, 1361 (1982).

[6]W. M. Saslow, Phys. Rev. B **27**, 588 (1983).

[7]N. Giordano, J. Low Temp. Phys. **55**, 495 (1984).

[8]M. Liu, Phys. Rev. B **29**, 2833 (1984).

[9]N. Giordano, in *Proceedings of the 17th Conference on Low Temperature Physics,* edited by U. Eckern, A. Schmid, W. Weber, and H. Wühl, (North-Holland, Amsterdam, 1984), p. 307.

[10]N. Giordano and P. Muzikar, in *Proceedings of the 17th Conference on Low Temperature Physics,* edited by U. Eckern, A. Schmid, W. Weber, and H. Wühl, (North-Holland, Amsterdam, 1984), p. 309.

[11]N. Giordano, J. Low Temp. Phys. **59**, 247 (1985).

[12]M. Grabinski and M. Liu, Phys. Rev. B **32**, 1856 (1985).

[13]G. Zimmermann and F. Pobell, J. Low Temp. Phys. **61**, 213 (1985).

[14]W. Zimmermann, Jr., Phys. Rev. B **33**, 139 (1986).

[15]N. Giordano and N. Edison, J. Low Temp. Phys. **64**, 29 (1986).

[16]H. A. Notarys, Phys. Rev. Lett. **22**, 1240 (1969).

[17]J. S. Langer and J. D. Reppy, in *Progress in Low Temperature Physics,* edited by C. J. Gorter (North-Holland, Amsterdam, 1970), Vol. VI.

[18]The importance of Poiseuille flow can be estimated from Eq. (61) of Ref. 7, which yields $v_n = v_m + R(\delta P_b - \delta P_c)$. The term involving R is due to Poiseuille flow, and it begins to become comparable to v_m only at the highest drive amplitudes used in Figs. 1 and 2, but never equals it. Thus it is reasonable to neglect Poiseuille flow in our calculations. It would, however, be straightforward to include these effects using the methods developed in Ref. 7.

[19]For data set A the magnitude of $v(t)$ increases approximately linearly with F, even when $w(t)$ varies nonlinearly. However, the relationship between $v(t)$ and F depends upon the values of the VST parameters which are assumed. For data set B it turns out that the magnitude of $v(t)$ increases with F much faster than linearly. This behavior can be understood quantitatively from a detailed consideration of (14). We thank M. Liu for pointing out how this behavior follows from (14).

[20]See for example, R. J. Donnelly, R. N. Hills, and P. H. Roberts, Phys. Rev. Lett. **42**, 725 (1979).

[21]One possible source of non-ideal behavior is the inevitable dust present in the backplate region (M. Liu, private communication). Near such pieces of dust the width of the backplate region will be much smaller than on average, and hence $\Delta L/L$ will be large in this vicinity. The aim of our work was to study the "ideal" behavior of VSTs, so effects of this sort were not considered. A quantitative study of effects such as these has not yet been performed, but would clearly be very interesting.